Noninvasive neuromagnetic single-trial analysis of human neocortical population spikes

Gunnar Waterstraat[a,1,2], Rainer Körber[b,1], Jan-Hendrik Storm[b], and Gabriel Curio[a,c]

[a]Neurophysics Group, Department of Neurology, Charité—Universitätsmedizin Berlin, 12203 Berlin, Germany; [b]Department of Biosignals, Physikalisch-Technische Bundesanstalt, 10587 Berlin, Germany; and [c]Bernstein Center for Computational Neuroscience, 10115 Berlin, Germany

Edited by Peter L. Strick, University of Pittsburgh, Pittsburgh, PA, and approved February 9, 2021 (received for review August 17, 2020)

Neuronal spiking is commonly recorded by invasive sharp microelectrodes, whereas standard noninvasive macroapproaches (e.g., electroencephalography [EEG] and magnetoencephalography [MEG]) predominantly represent mass postsynaptic potentials. A notable exception are low-amplitude high-frequency (~600 Hz) somatosensory EEG/MEG responses that can represent population spikes when averaged over hundreds of trials to raise the signal-to-noise ratio. Here, a recent leap in MEG technology—featuring a factor 10 reduction in white noise level compared with standard systems—is leveraged to establish an effective single-trial portrayal of evoked cortical population spike bursts in healthy human subjects. This time-resolved approach proved instrumental in revealing a significant trial-to-trial variability of burst amplitudes as well as time-correlated (~10 s) fluctuations of burst response latencies. Thus, ultralow-noise MEG enables noninvasive single-trial analyses of human cortical population spikes concurrent with low-frequency mass postsynaptic activity and thereby could comprehensively characterize cortical processing, potentially also in diseases not amenable to invasive microelectrode recordings.

magnetoencephalography | spiking activity | single-trial analysis | noninvasive | high-frequency somatosensory evoked responses

Neuronal activity can be measured at the level of single neurons using invasive microelectrode recordings reflecting both neuronal input (i.e., postsynaptic potentials) and neuronal output (i.e., action potentials or spikes). In contrast, at the population level, typical noninvasive macroelectrode recordings predominantly reflect mass neuronal input activity (1).

A notable exception to this methodological divide is macroscopic high-frequency activity: Concurrent microelectrode and macroelectrode recordings showed a relevant contribution of population spiking activity (i.e., neuronal output) to macroscopic neuronal fields (2, 3), especially at frequencies >500 Hz.

In consequence, macroscopic high-frequency oscillations (HFOs) have recently aroused interest, e.g., in the investigation of epilepsy and Parkinson's disease. In patients afflicted by epilepsy, electroencephalography (EEG) ripple and fast ripple oscillations were identified as biomarkers locating the seizure onset zone (4) and indicating the risk of epileptic seizures (5–7). In Parkinson's disease, cortical high-frequency potentials, evoked by deep brain stimulation in the subthalamic nucleus (STN), provide evidence for the activation of a "hyperdirect" pathway between STN and cortex (8), and spontaneous intra-STN HFOs were shown to be pathologically coupled to the phase of subcortical beta activity (9, 10). However, these data were captured mostly by invasive recordings or were limited to the frequency range <500 Hz.

So far, these restrictions are mainly due to the low signal-to-noise ratio (SNR) of HFOs >500 Hz. This is critical especially for noninvasive surface EEG or magnetoencephalography (EEG/MEG) since at frequencies >500 Hz signal amplitudes commonly fall below the intrinsic noise floor of standard EEG/MEG recording systems, precluding single-trial HFO analyses (11).

Here, high-frequency (~600 Hz) somatosensory evoked responses (hfSERs) (12), verified to correspond to single-trial spiking activity in neocortex by invasive recordings in macaque monkeys (13, 14), serve as HFO model in healthy humans. However, the standard approach to increase the SNR of hfSERs by averaging over approximately identical HFO occurrences (typically in the order of hundreds to thousands) precludes studying the natural variability inherent in brain function.

Addressing this issue, we demonstrate that an ultralow-noise MEG design (15, 16) enables noninvasive single-trial analyses of hfSERs. Exemplary proof-of-concept recordings in four healthy human subjects (17) revealed 1) a highly significant intertrial variability of hfSERs (i.e., neuronal output), which 2) is in the majority of subjects independent of the evoked low-frequency response (i.e., neuronal input), and 3) that hfSERs evoked by consecutive stimuli are mutually phase-correlated over several seconds. Thus, these measurements provide direct evidence that noninvasive ultralow-noise MEG recordings of macroscopic high-frequency responses enable time-resolved analyses of human cortical population spiking activity at the single-trial level.

Results

Ultralow-noise MEG recordings enabled the detection of evoked population spikes at an unprecedentedly high SNR in all four subjects, and, correspondingly, characteristic features are reported here at the single-subject level. A comparative full documentation of results from all subjects is included in *SI Appendix*.

Significance

Evolution has shaped the human brain as a "single-trial" processor reacting fast and reliably to environmental threats. The noninvasive analysis of its electrical activity commonly draws on electroencephalography/magnetoencephalography (EEG/MEG) with a millisecond time resolution suitable even for short-lived neuronal output spikes. However, while standard EEG/MEG can detect very small evoked population spikes, it does so only after averaging over hundreds of trials. Here, MEG based on an ultralow-noise superconducting quantum interference device (SQUID) is shown to enable the first noninvasive single-trial characterization of human cortical population spikes, revealing amplitudes highly variable between trials and intertrial correlated response latencies. Thus, by expanding the scope of noninvasive neurotechnology, ultralow-noise MEG can support single-trial analyses of input–output characteristics in the human brain.

Author contributions: G.W., R.K., J.-H.S., and G.C. designed research; G.W., R.K., J.-H.S., and G.C. performed research; R.K. and J.-H.S. contributed new reagents/analytic tools; G.W., R.K., and G.C. analyzed data; and G.W., R.K., J.-H.S., and G.C. wrote the paper.

The authors declare no competing interest.

This article is a PNAS Direct Submission.

[1]G.W. and R.K. contributed equally to this work.

[2]To whom correspondence may be addressed. Email: gunnar.waterstraat@charite.de.

This article contains supporting information online at https://www.pnas.org/lookup/suppl/doi:10.1073/pnas.2017401118/-/DCSupplemental.

Published March 11, 2021.

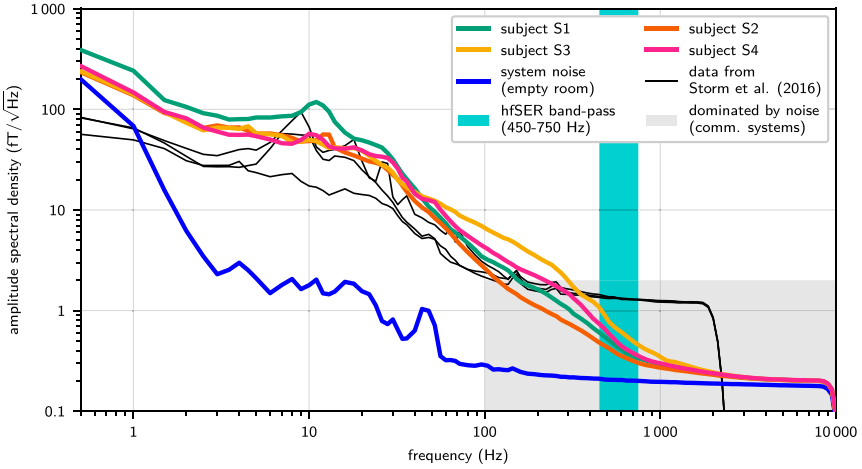

Fig. 1. Amplitude spectral density of resting-state recordings compared with system noise without subject. The system white noise level (blue line) in the empty magnetically shielded recording room was detected at 0.18 fT/$\sqrt{\text{Hz}}$, approximately one order of magnitude below the noise level of standard MEG systems. The gray shaded area indicates the range of frequencies and signal amplitudes dominated by system noise in case of a standard MEG system. Above 200 Hz (and extending through and even beyond the subsequently analyzed hfSER frequency band [cyan shading]), the ultralow-noise MEG still continued to show the physiological 1/*f*-spectral decay in resting-state recordings for all subjects (color-coded lines; cf. *Inset*) that in standard recordings would be hidden in system noise. The minute offset between system noise level and resting-state recordings persisting in the hf range (especially approximately >5,000 Hz) is mainly due to the natural thermal body noise (16, 21, 22). For a direct comparison, reanalyzed data from the immediate technological predecessor system (23) are shown featuring a high-frequency white magnetic field noise lower than commercial systems, but still obscuring biological activity at frequencies above 300 Hz (black lines; three subjects). The signal drop at 2,500 Hz is caused by low-pass filtering due to a lower sampling rate of the recordings (5,000 samples/s).

Spectral Density of Resting-State Recordings. Typical EEG/MEG-spectra exhibit a 1/*f* decay (18–20), asymptotically approaching the system noise floor at high frequencies. Accordingly, the transition of this 1/*f* decay into the spectrally flat white noise floor indicates the frequency boundary of visibility between recorded biological activity and system noise.

The white noise level of the custom-built ultralow-noise MEG system, measured in an empty magnetically shielded recording room, was 0.18 fT/$\sqrt{\text{Hz}}$ (Fig. 1). This is one order of magnitude below standard MEG systems (15) and close to the estimated thermal magnetic noise level of a living human body (16, 21, 22).

The MEG spectra of all four subjects recorded in a relaxed resting state (sensor positioned above the right lateral parietal region) were asymptotically approaching the system white noise level at frequencies >1,000 Hz. In consequence, in the frequency range of hfSERs (i.e., around 600 Hz), the ultralow-noise MEG system provided an unprecedented option for single-trial analyses of high-frequency MEG activity. This is highlighted by comparison with data obtained with the direct predecessor of the present MEG system (23). While this previous system already featured a white noise level lower than commercial systems, nonetheless in these data the 1/*f* trend of the spectrum, characteristic for neural activity, was superposed by system white noise at 300 Hz and above (cf. Fig. 1), rendering it impossible to record 600-Hz hfSERs at the single-trial level.

Analysis of Averaged hfSER Data. Single-channel MEG was recorded over the right parietal head (i.e., close to the hand area of the primary somatosensory cortex) during repetitive electrical median nerve stimulation at the contralateral left wrist at a stimulation rate of 3.27 /s. hfSERs were isolated, after removal of electrical stimulus artifacts via interpolation, by bandpass filtering (450 to 750 Hz) and subsequent averaging over 2,000 trials. In all four subjects, hfSERs clearly demonstrated evoked oscillatory burst activity centered at a latency of about 20 ms (Fig. 2 *A* and *B* and *SI Appendix*, Fig. A2). Filter ringing was excluded as relevant generator of hfSERs as the oscillatory peaks in the bandpass filtered data (Fig. 2*B*) could be distinguished also in the original wide-band data (Fig. 2*A*) as humps and notches on the ascending and descending slopes of the first (low-frequency) postsynaptic cortical component of the somatosensory evoked response peaking at 20 ms poststimulus latency ("N20m").

Complex-valued time–frequency (tf) decompositions permit a differentiation between phase-locked and phase-insensitive components of an evoked response (24, 25). The standard approach, i.e., averaging first over single trials (reducing both system noise and phase-jittered response components) and then calculating a tf decomposition, retains only the phase-locked response components in each tile of the tf plane. In contrast, the reverse order (first tf decomposition of single trials followed by within-tile averaging of the tf-resolved single-trial amplitudes) retains both phase-jittered components (i.e., its amplitude estimate is insensitive to the single-trial signal phase) and also system noise (the level of which is therefore decisive for the visibility of single-trial hfSER components).* Notably, even in the case of phase variability, phase-locked response components can be detected in the standard averaged response if the jitter is small relative to the cycle length of the oscillation or if the jitter occurs around a preferred phase. The relative contributions to phase-locked and phase-insensitive tf representations are determined by the stability of phases across trials relative to the cycle length at that frequency, the signal amplitude, and the SNR (24, 25).

In the present approach, hfSERs were detected in phase-locked (Fig. 2*C*) and, critically, also in the phase-insensitive (Fig. 2*D*) tf representations peaking at 400 to 2,000 Hz between 10 and 30 ms after stimulation. Phase-locked tf representations indicate that electric nerve stimulation elicited cortical population spikes at preferred latency modes in concordance with previous animal data (13, 14). Crucially, the significant phase-insensitive tf representations reveal that MEG recordings can detect hfSERs (phase-locked and/or phase-jittered components)

*The analysis steps identifying phase-locked and phase-insensitive hfSER activity match with the standard methodology to differentiate evoked and induced EEG/MEG activity (66, 67); however, the term "phase-insensitive" was preferred here to reflect the phase variability (latency jitter) observed in single trials for an evoked hfSER component (the mean of which appears as "phase-locked") rather than an independent induced oscillation.

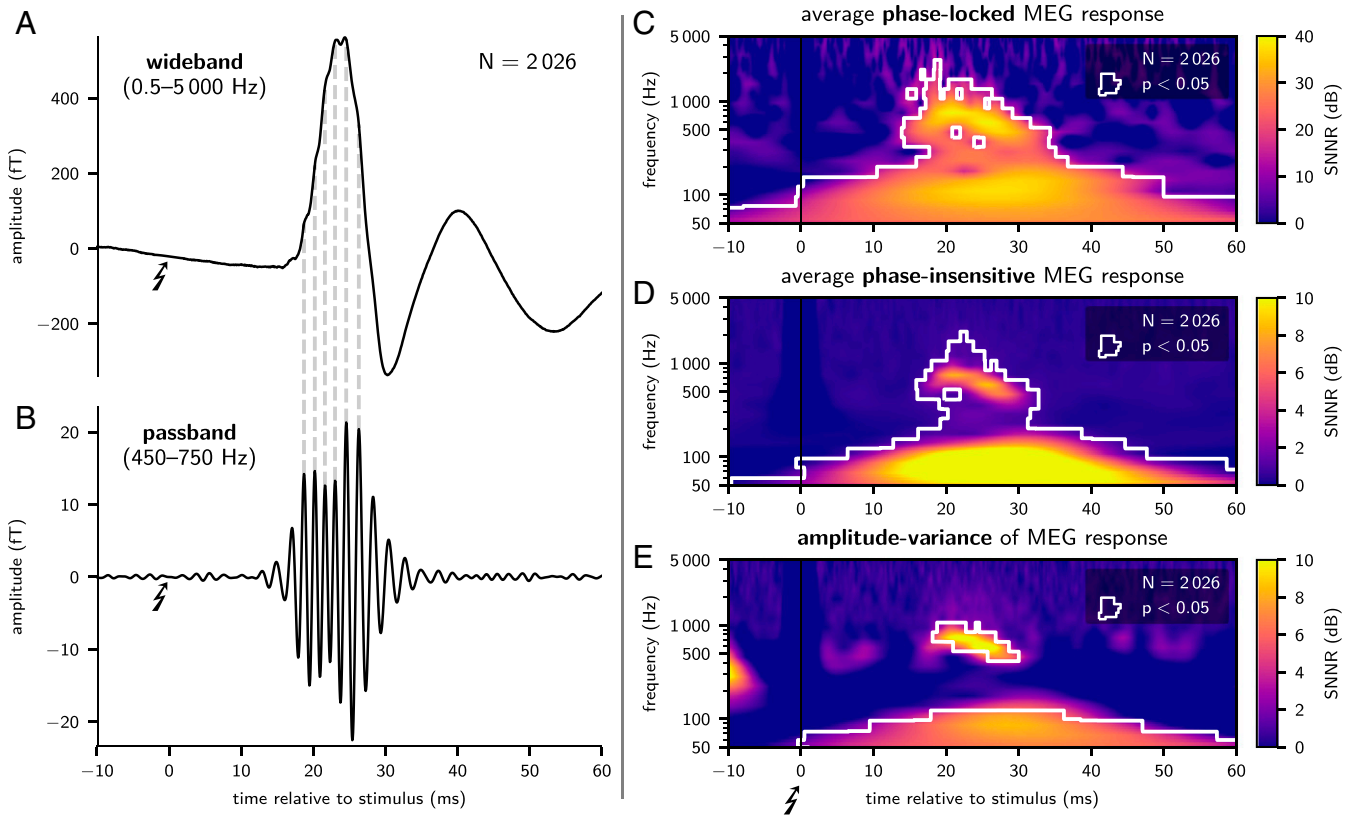

Fig. 2. Averaged somatosensory evoked responses (*A* and *B*), average phase-locked and phase-insensitive time–frequency (tf) representations of MEG responses (*C* and *D*), and analysis of excess variance in single-trial responses (*E*); exemplary data of subject S1. Wideband data (*A*) show the well-known rise to the first cortically evoked (low-frequency) postsynaptic component peaking at around 20 ms (N20m). Both the ascending and descending slopes of the N20m display humps and notches owing to superposition by low-amplitude high-frequency responses. This high-frequency somatosensory evoked response (hfSER) can be isolated as wavelet burst by phase-preserving bandpass filtering (*B*); dashed ancillary lines link original wideband humps with synchronous bandpassed wavelet peaks. The tf-resolved phase-locked MEG response (*C*) was calculated as tf transformation of the wideband data after averaging over trials. Thus, response components with variable phases between trials have been diminished by the averaging process. The phase-insensitive MEG response (*D*) was calculated as average of amplitudes of all tf-transformed single-trial responses. Amplitude-variance (*E*) was obtained as the variance of single-trial response amplitudes after tf transformation. For visualization, tf data were normalized independently in each frequency bin as signal-plus-noise-to-noise ratio (SNNR) (color-coded) by dividing the value in each tf tile by the mean prestimulus value at the respective frequency bin. Significant tf tiles are white-rimmed; *P* values were FWER-corrected.

even at the level of unaveraged single trials tainted by system noise (which, however, is exceptionally low for the present ultralow-noise MEG system). Corroborating previous human scalp-EEG recordings (24, 26), this detection of evoked ("added") hf-energy excludes a mere stimulus-driven phase reset of ongoing background HFO as sole generator of macroscopic hfSERs (25).

The increase of cortical population spiking activity evoked by median nerve stimulation was estimated as "signal-plus-noise"-to-noise ratio (SNNR: ratio of signal-plus-noise amplitudes in a response window to noise-only amplitudes in a prestimulus window): Phase-insensitive hfSER components had a single-trial SNNR between 5.6 dB (subject S4) and 8.8 dB (subject S1). The SNNR in the present ultralow-noise single-channel MEG recordings was therefore mostly higher than in optimally projected low-noise multichannel scalp-EEG recordings: In previous eight-channel EEG data, 9 of 10 subjects had a SNNR of hfSERs below 5.1 dB (26). Critically, the SNNR of phase-insensitive hfSER components is not obtained from a standard average across responses (as in, e.g., ref. 27) but is a ratio of average single-trial response powers (signal window/noise window). Accordingly, it is a direct representative of the single-trial SNNR and, in consequence, is decisive for the single-trial detectability of hfSERs (24). The present SNNR enabled an even more detailed analysis of intertrial response fluctuations of single-trial hfSERs, which showed that the variability of single-trial hfSERs significantly exceeded noise variability in all four subjects (Fig. 2*E* and *SI Appendix*, Fig. A2*E*).

The phase-locked components of the evoked response had a higher SNNR, remained visible at higher frequency bands, and were temporally more extended. This is mainly due to the attenuation of non–phase-locked noise and continuous EEG activity by averaging and expected from theoretical considerations of the SNR (24).

To assess the sensitivity of the ultralow-noise MEG approach for a single-trial hfSER characterization, the overlap of signal strength distributions in the response time window (15 to 35 ms) and in a prestimulus time window devoid of stimulus-elicited burst activity (−35 to 15 ms) was determined for each subject: Depending on the individual SNR, single-trial hfSERs' strength variability could be differentiated from noise contributions (*SI Appendix*, Fig. S1).

Analysis of Single-Trial hfSERs. Graphical single-trial representations (Fig. 3 and *SI Appendix*, Fig. A3) of bandpass-filtered responses (450 to 750 Hz) clearly depicted single-trial hfSERs as can be seen by the temporal alignment of wave peaks and troughs forming vertically oriented band structures at latencies around 20 ms poststimulus and by the increase of single-trial signal amplitudes during the response time interval. A complementary analysis, representing amplitude and phase of single-trial data

points (obtained by Hilbert transformation) in polar coordinates, showed a fixed phase relation of single-trial hfSERs to a 600-Hz sinusoid and an amplitude larger than in a later (noise-only) analysis window (*SI Appendix*, Fig. S2). Moreover, these ultralow-noise MEG recordings of single-trial hfSERs were instrumental to demonstrate a significant hf-response variability with partial amplitude reduction of evoked activity over several trials and slow fluctuations of response peak latencies.

Building on this MEG single-trial capability, the newly uncovered response variability was subjected to further analysis. In a first step, hfSERs were related to concomitant low-frequency evoked responses by sorting all single hfSER trials according to their root-mean-square (rms) amplitude. In a second step, a complementary analysis was performed by sorting according to the latency of the low-frequency N20m response.

These analyses showed a functional dissociation between the first intracortical postsynaptic response to thalamocortical input (i.e., the low-frequency N20m) and the variability of the population spike response strength and latency (i.e., hfSER amplitude and phase) as detected noninvasively at the macroscopic level: In all subjects, response amplitudes in the two frequency bands were neither correlated in single trials nor after creation of subaverages ($n = 50$; Fig. 4 and *SI Appendix*, Fig. A4). Analyzing the relation between latencies of the low-frequency and the burst response yielded no significant results in the present dataset (*SI Appendix*, Fig. S3).

This raises the interesting possibility that the single-trial high-frequency population spike response is not solely controlled by thalamocortical input, but rather might reflect a variable local network state.

In a third step, the autocorrelation of hfSERs across trials was analyzed to investigate temporal fluctuations of cortical excitability. For formalized testing of the autocorrelation across multiple lags, the autocorrelation function (acf) of hfSERs across trials was condensed to its integral; this was calculated independently for the instantaneous amplitude and phase of the analytic signal of single-trial hfSERs, obtained by Hilbert transformation (*SI Appendix*, Fig. S4). In three of four subjects, hfSERs showed significantly increased autocorrelation of phases. Partial autocorrelation (i.e., correlation controlled for the effect of intermediate trials) indicated that the phases of hfSERs were correlated across as many as 40 consecutive trials (corresponding to >10 s at a stimulation frequency of 3.27 /s). Only in the subject with the lowest SNNR (subject S4), this effect was not observed, consistent with a possible type II error.

Only in one subject (subject S2; cf. *SI Appendix*, Fig. S4), hfSERs additionally showed an increased autocorrelation of instantaneous signal amplitudes. Accordingly, while autocorrelation of instantaneous amplitudes across trials might be of physiological relevance, it appears to be less pronounced than the autocorrelation of phases.

Comparison with Data Obtained at Higher System Noise. To assess the noise level required for single-trial analyses, hfSERs were also analyzed for MEG data obtained using the immediate technical predecessor of the present system, operating at 1.28 $\mathrm{fT}/\sqrt{\mathrm{Hz}}$ system noise levels (23). Here, while phase-locked hfSER response components were detected in two of three subjects, phase-jittered hfSER components (i.e., amplitude increases at the single-trial level) were not detected in any of these recordings. In consequence, single-trial analyses of hfSERs conducted in these data revealed negative results altogether. These data are described in detail in *SI Appendix*, *Supplementary Material*.

Discussion

In this study, human cortical population spikes were recorded noninvasively using ultralow-noise MEG. hfSERs were examined as a well-studied example of cortical population spikes (13, 14) so that established techniques in the study of evoked responses could be extended and blended into single-trial analysis techniques.

Four major results were obtained: 1) As a technical prerequisite, we demonstrated that noninvasive ultralow-noise MEG recordings can discriminate ongoing (unaveraged) biomagnetic activity against concurrent system noise even in the high-frequency range up to at least 1,000 Hz. This unprecedented sensitivity is based on a recent leap in the development of MEG sensors (15, 16) that reduced the system white noise by about one order of

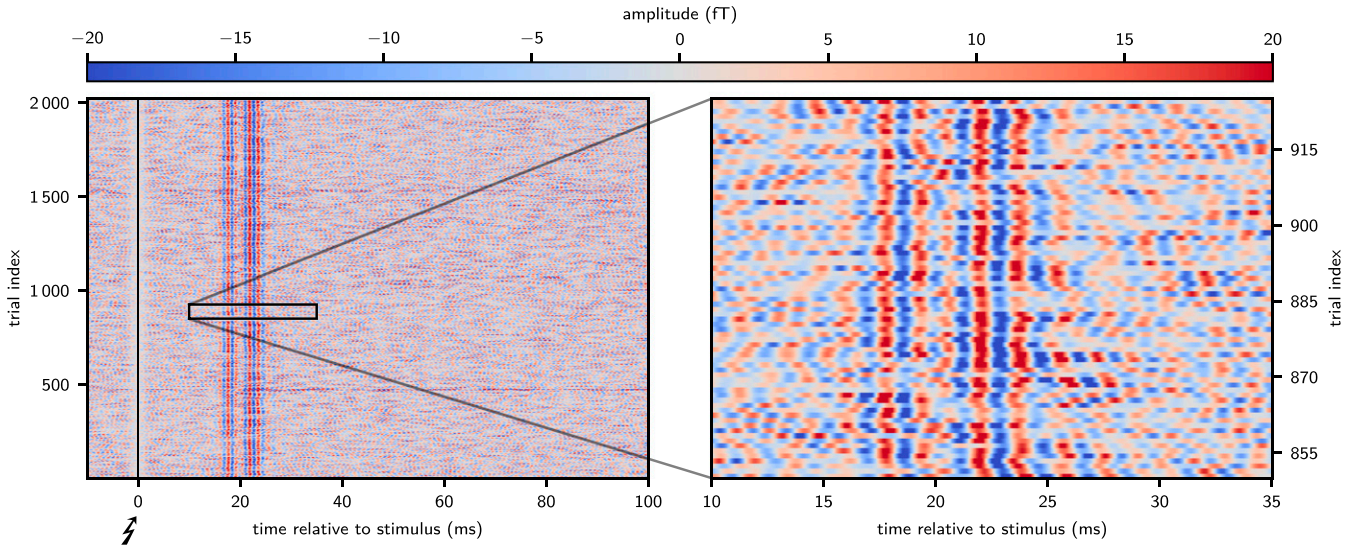

Fig. 3. Time-amplitude resolved detection of single-trial hfSERs; exemplary data of subject S2. Single trials after bandpass filtering (450 to 750 Hz) were vertically stacked in chronological order with amplitudes coded in color saturation. The alignment of single-trial phases is clearly visible as formation of vertically oriented bands in the response time window 15 to 30 ms (*Left*). Furthermore, increased color saturation in that window indicates larger single-trial amplitudes of hfSERs in relation to noise. The magnification of a figure section (*Right*) was prepared avoiding any graphical interpolation [since this would implicitly result in a (sub)average over trials]. These data reveal a significant variability of single-trial burst responses, e.g., partial reduction of high-frequency responses across several trials and slow fluctuations of latencies.

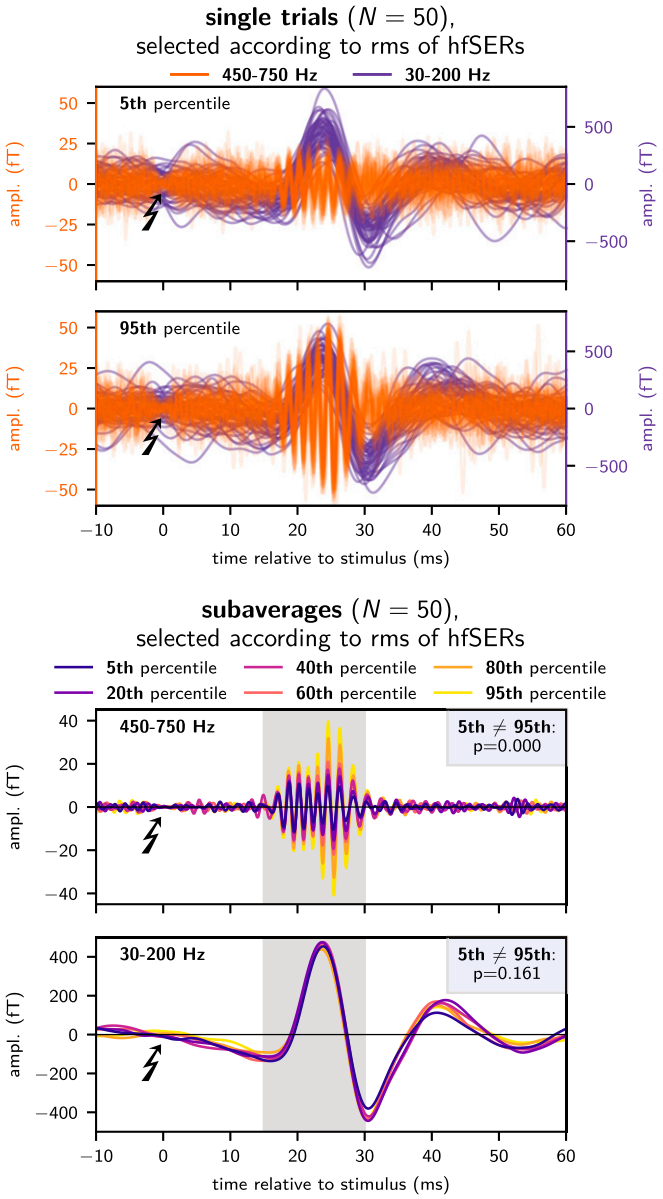

Fig. 4. Relation between hfSERs and low-frequency evoked responses; exemplary data of subject S1. Trials were sorted according to the rms amplitude of single-trial hfSERs. This procedure clearly differentiated between weak (5th percentile) and strong (95th percentile) hfSERs while the noise level remained approximately constant. Notably, concurrently evoked low-frequency components of single-trial responses were approximately equal for weak and strong hfSERs (*Top*). This was corroborated by forming percentile-specific subaverages (*Bottom*) of low-frequency responses, which were equal despite a clear gradual recruitment of hfSER subaverages underlining the effectiveness of the single-trial sorting.

magnitude in comparison with presently available standard systems. A complementary reanalysis of MEG data obtained with the immediate technological predecessor showed that the lower SNR provided by this system precluded the single-trial detection of hfSERs. 2) We demonstrated that these ultralow-noise single-channel MEG recordings of hfSERs are superior in SNR when compared with optimal spatial projections of multichannel low-noise EEG. 3) This allowed uncovering a previously unknown amplitude variability of single-trial hfSERs (at constant stimulation intensity), which was shown to be functionally decoupled from the underlying low-frequency response. This finding provides noninvasive evidence that—while driven by the same input (28)—low- and high-frequency response channels at the macroscopic level are generated by different mechanisms. 4) Phases (i.e., latencies) of hfSERs were found autocorrelated across trials, and accordingly, their variability is nonrandom. Remarkably, the presented results were statistically robust within single subjects, and, in line with previous findings, variations in results can be traced back to interindividually different SNNRs. Providing an estimate of these differences across subjects, averaged hfSER responses of variable strength were detectable in up to 80% in a larger cohort of 49 subjects (29), and this variability is covered also in the present set of subjects.

Notably, hfSERs are not related to ringing artifacts resulting from bandpass filtering of sharp transients since they can be identified already in the wideband signal as humps and notches superimposed on the low-frequency response (Fig. 2 *A* and *B*). Furthermore, hfSERs demonstrate a clearly delineated peak at around 600 Hz in their instantaneous power spectrum with an energy trough at lower frequencies (Fig. 2*D*), a feature that also discriminates epileptic HFOs and spike-like artifacts (30, 31). Moreover, the electromagnetic field distribution of hfSERs has a characteristic evolution from an early monopolar pattern (visible in EEG) to later dipolar patterns [visible in both EEG and MEG (12, 32, 33)], which can be modeled by a response propagation from the thalamus via thalamocortical fibers to the primary somatosensory cortex (29, 34).

Crucially, it has been shown earlier that macroscopic hfSERs, indeed, correspond to distinct single-cell burst patterns (14), and, accordingly, extending recent epicortical microelectrode recordings of single-unit spiking (35) and epicortical ("mesoscale") recordings (36) of correlated action potentials to a noninvasive macroscopic regimen, the present ultralow-noise MEG recordings of single-trial high-frequency activity represent a noninvasive measure of cortical population spikes.

An approximate estimate of the number of cortical neurons contributing to the evoked hfSERs can be derived from two converging findings: First, the source strength (dipole moment) of human hfSERs evoked by median nerve stimulation amounts to about 1.2 nAm, as determined in independent studies (33, 37). Second, based on realistically shaped three-dimensional multicompartment single-neuron models, a mean dipole moment of about 1 pAm was estimated for a sodium spike generated in principal cortical neurons (38). Taken together, these findings predict a contribution from an ensemble of about 1,200 neurons to human cortical population spikes observed noninvasively as hfSERs after median nerve stimulation.

Spike bursts in thalamocortical relay neurons can be elicited by changes in stimulus intensity (39) and might represent a "wake-up call" for rare events (40). In this context, one might argue that hfSERs are merely signaling the unnaturally massive input due to electrical nerve stimulation; however, it has been shown that natural "tapping" stimuli, placed in the receptive field of single neurons that showed burst responses to electric median nerve stimuli, elicit spike bursts (13) as well.

The finding of nonrandom variability of macroscopic population spike bursts corroborates the interpretation of physiological significance of neuronal bursting activity: The precise number and timing of spikes within a burst could serve as an additional information channel in the communication between neurons (41, 42). This has been demonstrated in the somatosensory system of the weakly electric fish where bursting activity was shown to represent a robust signal that is transmitted in parallel to spiking activity and provides evidence about distinct stimulus features (43).

Nonrandom phase variations in the macroscopic hfSERs indicate structured trial-to-trial latency shifts in the population spike responses. Covariations between the response latencies of cortical neurons was previously shown to enable perceptual binding

and to promote stimulus-feature selectivity (44). A precise (i.e., nonrandom) timing of cortical bursting activity in the somatosensory barrel cortex of rats also suggested that hfSERs can define a temporal reference frame for subsequent processing (45). Accordingly, the presence of structured autocorrelation in the phases of the macroscopic hfSERs underscores that bursting activity does not only signal the binary information about the presence/absence of somatosensory input but could carry additional information that can be addressed in future studies, concerning, e.g., possible drifts in arousal, attention, subject movements, or endogenous ultraslow (0.1-Hz) rhythms (46, 47).

Critically, the present approach provides a robust recipe for progress in the overarching paradigm that noninvasive low-noise macrosensor recordings of neuronal activity can enable the simultaneous study of both slow responses representing mass postsynaptic potentials and high-frequency activity corresponding to evoked cerebral population spikes at the single-subject single-trial level. While this paradigm is open to MEG as well as EEG, single-channel ultralow-noise MEG outperformed previously unrivaled multichannel EEG recordings. Additionally, the future option of multichannel ultralow-noise MEG systems is a straightforward perspective for further SNR improvements by the application of spatial projection techniques, custom-tailored to spontaneous neuronal oscillations (48) or high-frequency evoked responses (49).

With regard to pathological oscillations, high-frequency activity has been shown to be involved in the pathophysiology of Parkinson's disease (50) and as a potential biomarker of epilepsy (5). Correspondingly, low-noise recordings may extend our knowledge about the significance of high-frequency activity to clinical symptoms by improving the SNR in the high-frequency range (31). Furthermore, high-frequency activity in these diseases had been revealed mainly by invasive recordings during deep brain stimulation or epilepsy surgery. The availability of noninvasive, low-noise, high-frequency recordings will permit studying whether other brain pathologies not amenable to invasive brain recordings are related to pathologic dynamics in high-frequency activity as well.

Furthermore, single-trial analysis of electrophysiological data is aligning the algorithmic pipeline to the natural operating mode of the brain, which is processing and responding to single stimuli in real time (51). Specifically, averaging across responses cannot capture the dynamics of single-trial responses and might even lead to misinterpretations (52). In this regard, statistical methods were developed to accurately delineate the timing of neuronal activity during single trials (53–55). Notably, however, these single-trial analyses became possible only via the high SNR provided by invasive electrocorticography.

The presented MEG approach to noninvasive single-trial analysis of population spikes can thus benefit the investigation of human neurophysiology and brain pathology; e.g., it could provide insights into how cortical input (low frequency) is transformed to cortical output (high frequency) at the macroscopic level and thereby provide a significant refinement of the neuroscientific toolbox for studying human cortical neurophysiology.

Methods

Subjects. Recordings were acquired in four healthy male participants (age, 34 to 60 y). The subjects were informed about the experiment and gave consent to participate. The full study protocol has been approved by the Ethics Committee of the Physikalisch-Technische Bundesanstalt (ID: 1/15).

MEG Equipment. Incremental technological improvements have successively lowered the field noise of low-Tc superconducting quantum interference device (SQUID)-based MEG systems (56–58). Here, a recently developed (15, 16) ultralow-noise single-channel first-order axial gradiometer setup is used (120-mm baseline; 45-mm pick-up coil diameter). Utilizing aluminized polyester as superinsulation and aluminum-oxide as heat shields (59) for the low intrinsic noise Dewar 2 (LINOD2) rendered the Dewar noise negligible. In this gradiometric configuration, a total measurement noise level of about 0.18 $fT/\sqrt{Hz}$ (referred to the bottom pick-up loop) was achieved—an order of magnitude below presently available standard systems. The system was operated at the center of a moderately magnetically shielded room consisting of two layers of mu-metal and one eddy current layer ("Zuse-MSR"). MEG signals were recorded at a sampling rate of 20 kHz with a 24-bit digitizer.

MEG Recordings. For benchmarking, a first recording was done with the system set up inside the otherwise empty shielded room (i.e., without a subject).

Subsequently, subjects laid sideways on a wooden rack at the center of the shielded room with the right side of their heads facing upward. The participant's head was cast in a molded vacuum cushion in order to minimize any movements. The Dewar—containing the SQUID—was placed above the head with the bottom side of the Dewar directly hovering over the head area above the approximate lateral field maximum of the activated hand region of the right somatosensory cortex. In consequence, the total distance between the MEG pick-up coil and the head surface amounted to 13 to 14 mm.

The subjects were asked to relax—especially the musculature of the face, jaw, and shoulders—and to remain still. Subjects were covered by a blanket to ensure comfort, and—during median nerve stimulation (described below)—to sustain normal peripheral body temperature for constant and rapid peripheral nerve conduction velocity. Eyes-open resting-state MEG (i.e., without median nerve stimulation) was subsequently recorded for a duration of 10 min.

In order to record hfSERs, the left median nerve was stimulated at a repetition rate of 3.27 /s (0.2-ms monophasic square wave pulses) and at a constant current intensity of 1.5× above motor threshold, such that a clear twitch of the thumb was visible for every stimulus. hfSER recordings lasted for about 10 min, permitting to record ∼2,000 trials. The MEG data during median nerve stimulation were recorded continuously at full bandwidth (0 to 8,000 Hz) and processed off-line.

To assess the advantage of the ultralow-noise MEG sensor over previous recordings, data from ref. 23 were reanalyzed. In that study, the direct predecessor of the present MEG system was used to record hfSERs during 9-Hz median nerve stimulation in three subjects (including subjects S3 and S4 of the present study). While the white noise spectral density of 1.28 $fT/\sqrt{Hz}$ of that device was lower in comparison with commercially available MEG systems, it was about 7× higher than in the present system. Additionally, with the sensor contained in a commercial dewar, the warm–cold distance of ∼28 mm was about twice the distance of the present ultralow-noise MEG system. A description of the technical details and the measurement procedures of the data (23) is given together with the results in *SI Appendix*. Apart from shorter temporal analysis windows owing to the shorter interstimulus intervals, the data were subsequently analyzed in exactly the same manner as for the present study.

Spectral Density Estimation of Resting-State Recordings. A modified Welch's averaged periodogram technique (60) was used to obtain a robust estimate of the amplitude spectral density of the resting-state recordings. As in Welch's original method, periodograms were obtained from shorter data segments and averaged to obtain an estimate of the spectral density of the entire dataset. However, in order to be robust against corrupted segments of data (e.g., due to movement or muscle activity), we calculated the trimmed mean over all subperiodograms, such that at every frequency only the central 60% of power values were averaged.

Furthermore, to enable a smooth visualization of the spectral density at logarithmically scaled frequencies, spectral densities were estimated independently in 11 bands of logarithmically increasing width and with decreasing resolution at increasing frequencies, and were joined subsequently.

Analysis of Averaged hfSER Data. In order to visualize the average evoked response to median nerve stimulation, data were filtered in two bands: 0.5 to 5,000 Hz ("wideband") and 450 to 750 Hz ("passband"). To avoid ringing of the applied digital filters, the stimulation artifact was removed by monotone cubic hermite spline interpolation in the interval [−2, 2 ms) around the stimulus (49). Butterworth type IIR filters of order 3 were applied in forward and backward direction to prevent signal distortion and to obtain unchanged latencies ("zero phase response").

Differentiating between phase-locked ("evoked") and phase-jittered ("induced") components of the evoked responses is possible using a tf transformation (24, 61): Let $x_i(t)$ denote the MEG signal at time t in trial i of

N total trials. The tf-resolved instantaneous amplitude of the average evoked response: $\left|TF(\sum_{i=1}^{N} x_i(t)/N)\right|$, with $|TF(\cdot)|$ denoting the modulus of the complex-valued tf transformation, is sensitive mainly to at least partially phase-locked evoked components since components with randomly distributed ("jittered") phases would be attenuated by averaging over trials, as would be system noise. On the other hand, the average of the tf-resolved instantaneous single-trial amplitudes $\sum_{i=1}^{N}|TF(x_i(t))|/N$ is phase-insensitive and can be used as a measure to estimate the single-trial SNNR of phase-locked and phase-jittered components of the evoked response. Here, as tf transform, the generalized Fourier transform (GFT) (62, 63) was chosen due to its property of generating a complex-valued tf representation with absolute reference to phase and custom tiling of the tf plane. This possibility allows to balance the conflicting requirements of fine-graded tf resolution and computer-memory efficiency. Specifically, the tf plane was tiled into 30 logarithmically increasing frequency bands between 5 and 5,000 Hz with a frequency-specific sampling rate of four samples per period. The GFT was calculated from the single-trial wideband data in the [−60, 160 ms) window around every stimulus ([−10, 60 ms) for the reanalysis of the data from ref. 23, respectively). The phase-locked and phase-insensitive tf representations of MEG responses were standardized as SNNR using division by the average noise amplitude in every frequency band, obtained by tf transformation of prestimulus data in the window (−220, −10 ms) prior to the stimulus ([−80,−10 ms) for the reanalysis of the data from ref. 23, respectively). We are aware of the partial overlap of the defined signal window and prestimulus window at the given interstimulus interval. However, while the interest of the analysis was focused on the nonoverlapping poststimulus interval, extended prestimulus and poststimulus segments in the signal window were included to assert that the evoked components showed the temporally expected rise and return to baseline activity.

Significance testing for phase-locked and phase-insensitive tf representations of evoked responses was done using a Studentized bootstrap test for the difference of means (64) between the tf transformations obtained from the signal window and prestimulus window. The family-wise error rate (FWER) was controlled using a bootstrap procedure taking into account the interdependence between the individual tf tiles of the GFT data (65).

To quantify the excess variability of hfSERs over noise, the tf resolved variance of single-trial amplitudes was obtained as $var_{i...N}(|TF(x_i(t))|)$, where $var_{i...N}(\cdot)$ denotes the variance calculated across trials, and divided by the frequency-wise average variance of single-trial amplitudes in the prestimulus noise window defined above. Significance testing was performed by bootstrap-resampling (1,000 times) of the instantaneous single-trial amplitudes $|TF(x_i(t))|$ in the analyzed tf tile and the prestimulus window and FWER correction using the same method as above.

Analysis of Single-Trial hfSERs. For the visual assessment of single-trial hfSERs, the evoked responses of individual subjects were represented as two-dimensional maps with time as abscissa, trial-index as ordinate axis, and polarity-specific hfSER amplitudes coded by color saturation. Special care was taken to disable any explicit or implicit averaging by graphical interpolation, due to either software or insufficient image resolution. This is of paramount importance since plotting with interpolated hue and color saturation (as is frequently done to reduce aliasing and to increase the smoothness of printed or on-screen images) or insufficient resolution would obfuscate the targeted veridical depiction of single-trial hfSERs. Eventually, this graphical representation allows for an immediate assessment of the variability of the signal and of a potential mutual interdependence of sequential single-trial responses.

To investigate the relation between the low-frequency response and hfSERs, trials were sorted according to the single-trial rms amplitude of hfSERs and, for a separate analysis, also according to the latencies of the low-frequency N20m. Trials with an rms amplitude of the single-trial hfSER above or below the median ±1.5× IQR were excluded from the analysis.

Subaverages of $N = 50$ trials—consecutive in the order of the respective sorting—at increasing percentiles were obtained for a low-frequency passband (30 to 200 Hz) and the high-frequency passband (450 to 750 Hz). Differences between the subaverages at the lowest and the highest percentile were tested by a bootstrapped summed t statistic for the temporal response window [15, 30 ms).

The variability of single-trial hfSERs was further characterized by an analysis of autocorrelation between responses. Details of the analysis are described in *SI Appendix*.

Data Availability. All analyses were performed in the Python programming language in its most recent version (3.8.2) relying on the additional packages numpy (1.18.2), scipy (1.4.1), matplotlib (3.2.1), and the author-made M/EEG-analysis package "meet" in its most recent version (https://github.com/neurophysics/meet). The code generated during this study and the anonymized full dataset supporting the current study has been deposited in the online repository https://gin.g-node.org/gwaterst/2021-hfMEG (17) (access to the raw data will be granted by the authors upon reasonable request to the corresponding author).

ACKNOWLEDGMENTS. G.W. and G.C. are supported in part by Deutsche Forschungsgemeinschaft (German Research Foundation) Project ID 424778381 TRR 295.

1. Y. C. Okada, J. Wu, S. Kyuhou, Genesis of MEG signals in a mammalian CNS structure. *Electroencephalogr. Clin. Neurophysiol.* **103**, 474–485 (1997).
2. M. A. Belluscio, K. Mizuseki, R. Schmidt, R. Kempter, G. Buzsáki, Cross-frequency phase–phase coupling between theta and gamma oscillations in the hippocampus. *J. Neurosci.* **32**, 423–435 (2012).
3. B. Teleńczuk, S. N. Baker, R. Kempter, G. Curio, Correlates of a single cortical action potential in the epidural EEG. *Neuroimage* **109**, 357–367 (2015).
4. J. Jacobs *et al*., High-frequency oscillations (HFOs) in clinical epilepsy. *Prog. Neurobiol.* **98**, 302–315 (2012).
5. M. Zijlmans *et al*., High-frequency oscillations as a new biomarker in epilepsy. *Ann. Neurol.* **71**, 169–178 (2012).
6. P. Jiruska *et al*., Update on the mechanisms and roles of high-frequency oscillations in seizures and epileptic disorders. *Epilepsia* **58**, 1330–1339 (2017).
7. B. Frauscher *et al*., High-frequency oscillations: The state of clinical research. *Epilepsia* **58**, 1316–1329 (2017).
8. S. Miocinovic *et al*., Cortical potentials evoked by subthalamic stimulation demonstrate a short latency hyperdirect pathway in humans. *J. Neurosci.* **38**, 9129–9141 (2018).
9. A. I. Yang, N. Vanegas, C. Lungu, K. A. Zaghloul, Beta-coupled high-frequency activity and beta-locked neuronal spiking in the subthalamic nucleus of Parkinson's disease. *J. Neurosci.* **34**, 12816–12827 (2014).
10. J. López-Azcárate *et al*., Coupling between beta and high-frequency activity in the human subthalamic nucleus may be a pathophysiological mechanism in Parkinson's disease. *J. Neurosci.* **30**, 6667–6677 (2010).
11. H. J. Scheer, T. Sander, L. Trahms, The influence of amplifier, interface and biological noise on signal quality in high-resolution EEG recordings. *Physiol. Meas.* **27**, 109–117 (2006).
12. G. Curio *et al*., Localization of evoked neuromagnetic 600 Hz activity in the cerebral somatosensory system. *Electroencephalogr. Clin. Neurophysiol.* **91**, 483–487 (1994).
13. S. N. Baker, G. Curio, R. N. Lemon, EEG oscillations at 600 Hz are macroscopic markers for cortical spike bursts. *J. Physiol.* **550**, 529–534 (2003).
14. B. Telenczuk, S. N. Baker, A. V. M. Herz, G. Curio, High-frequency EEG covaries with spike burst patterns detected in cortical neurons. *J. Neurophysiol.* **105**, 2951–2959 (2011).
15. J.-H. Storm, P. Hömmen, D. Drung, R. Körber, An ultra-sensitive and wideband magnetometer based on a superconducting quantum interference device. *Appl. Phys. Lett.* **110**, 072603 (2017).
16. J.-H. Storm, P. Hömmen, N. Höfner, R. Körber, Detection of body noise with an ultra-sensitive SQUID system. *Meas. Sci. Technol.* **30**, 125103 (2019).
17. G. Waterstraat, R. Körber, J.-H. Storm, G. Curio, Noninvasive neuromagnetic single-trial analysis of human neocortical population spikes; MEG data and scripts. German Neuroinformatics Node. https://gin.g-node.org/gwaterst/2021-hfMEG. Deposited 22 February 2021.
18. C. Bédard, H. Kröger, A. Destexhe, Does the 1/*f* frequency scaling of brain signals reflect self-organized critical states? *Phys. Rev. Lett.* **97**, 118102 (2006).
19. K. J. Miller, L. B. Sorensen, J. G. Ojemann, M. den Nijs, Power-law scaling in the brain surface electric potential. *PLOS Comput. Biol.* **5**, e1000609 (2009).
20. W. S. Pritchard, The brain in fractal time: 1/*f*-like power spectrum scaling of the human electroencephalogram. *Int. J. Neurosci.* **66**, 119–129 (1992).
21. W. Myers *et al*., Calculated signal-to-noise ratio of MRI detected with SQUIDs and Faraday detectors in fields from 10 microT to 1.5 T. *J. Magn. Reson.* **186**, 182–192 (2007).
22. T. Varpula, T. Poutanen, Magnetic field fluctuations arising from thermal motion of electric charge in conductors. *J. Appl. Phys.* **55**, 4015–4021 (1984).
23. J.-H. Storm, D. Drung, M. Burghoff, R. Körber, A modular, extendible and field-tolerant multichannel vector magnetometer based on current sensor SQUIDs. *Supercond. Sci. Technol.* **29**, 094001 (2016).
24. G. Waterstraat *et al*., Are high-frequency (600 Hz) oscillations in human somatosensory evoked potentials due to phase-resetting phenomena? *Clin. Neurophysiol.* **123**, 2064–2073 (2012).
25. P. Sauseng *et al*., Are event-related potential components generated by phase resetting of brain oscillations? A critical discussion. *Neuroscience* **146**, 1435–1444 (2007).

26. G. Waterstraat, M. Scheuermann, G. Curio, Non-invasive single-trial detection of variable population spike responses in human somatosensory evoked potentials. *Clin. Neurophysiol.* **127**, 1872–1878 (2016).
27. J. F. Barry *et al*., Optical magnetic detection of single-neuron action potentials using quantum defects in diamond. *Proc. Natl. Acad. Sci. U.S.A.* **113**, 14133–14138 (2016).
28. F. Klostermann, G. Nolte, F. Losch, G. Curio, Differential recruitment of high frequency wavelets (600 Hz) and primary cortical response (N20) in human median nerve somatosensory evoked potentials. *Neurosci. Lett.* **256**, 101–104 (1998).
29. P. Ritter, F. Freyer, G. Curio, A. Villringer, High-frequency (600 Hz) population spikes in human EEG delineate thalamic and cortical fMRI activation sites. *Neuroimage* **42**, 483–490 (2008).
30. S. Burnos *et al*., Human intracranial high frequency oscillations (HFOs) detected by automatic time-frequency analysis. *PLoS One* **9**, e94381 (2014).
31. T. Fedele *et al*., Prediction of seizure outcome improved by fast ripples detected in low-noise intraoperative corticogram. *Clin. Neurophysiol.* **128**, 1220–1226 (2017).
32. T. Fedele *et al*., Towards non-invasive multi-unit spike recordings: Mapping 1kHz EEG signals over human somatosensory cortex. *Clin. Neurophysiol.* **123**, 2370–2376 (2012).
33. I. Hashimoto, T. Mashiko, T. Imada, Somatic evoked high-frequency magnetic oscillations reflect activity of inhibitory interneurons in the human somatosensory cortex. *Electroencephalogr. Clin. Neurophysiol.* **100**, 189–203 (1996).
34. R. Gobbelé *et al*., Different origins of low- and high-frequency components (600 Hz) of human somatosensory evoked potentials. *Clin. Neurophysiol.* **115**, 927–937 (2004).
35. D. Khodagholy *et al*., NeuroGrid: Recording action potentials from the surface of the brain. *Nat. Neurosci.* **18**, 310–315 (2015).
36. T. Bockhorst *et al*., Synchrony surfacing: Epicortical recording of correlated action potentials. *Eur. J. Neurosci.* **48**, 3583–3596 (2018).
37. G. Curio *et al*., Somatotopic source arrangement of 600 Hz oscillatory magnetic fields at the human primary somatosensory hand cortex. *Neurosci. Lett.* **234**, 131–134 (1997).
38. S. Murakami, Y. Okada, Contributions of principal neocortical neurons to magnetoencephalography and electroencephalography signals. *J. Physiol.* **575**, 925–936 (2006).
39. K. Funke, N. Kerscher, High-frequency (300–800 Hz) components in cat geniculate (dLGN) early visual responses. *J. Physiol. Paris* **94**, 411–425 (2000).
40. S. M. Sherman, Tonic and burst firing: Dual modes of thalamocortical relay. *Trends Neurosci.* **24**, 122–126 (2001).
41. E. M. Izhikevich, N. S. Desai, E. C. Walcott, F. C. Hoppensteadt, Bursts as a unit of neural information: Selective communication via resonance. *Trends Neurosci.* **26**, 161–167 (2003).
42. H. G. Eyherabide, A. Rokem, A. V. M. Herz, I. Samengo, Bursts generate a non-reducible spike-pattern code. *Front. Neurosci.* **3**, 8–14 (2009).
43. M. G. Metzen, R. Krahe, M. J. Chacron, Burst firing in the electrosensory system of gymnotiform weakly electric fish: Mechanisms and functional roles. *Front. Comput. Neurosci.* **10**, 81 (2016).
44. P. Fries, S. Neuenschwander, A. K. Engel, R. Goebel, W. Singer, Rapid feature selective neuronal synchronization through correlated latency shifting. *Nat. Neurosci.* **4**, 194–200 (2001).
45. D. S. Barth, Submillisecond synchronization of fast electrical oscillations in neocortex. *J. Neurosci.* **23**, 2502–2510 (2003).
46. A. Rayshubskiy *et al*., Direct, intraoperative observation of ~0.1 Hz hemodynamic oscillations in awake human cortex: Implications for fMRI. *Neuroimage* **87**, 323–331 (2014).
47. V. V. Nikulin *et al*., Monochromatic ultra-slow (~0.1 Hz) oscillations in the human electroencephalogram and their relation to hemodynamics. *Neuroimage* **97**, 71–80 (2014).
48. V. V. Nikulin, G. Nolte, G. Curio, A novel method for reliable and fast extraction of neuronal EEG/MEG oscillations on the basis of spatio-spectral decomposition. *Neuroimage* **55**, 1528–1535 (2011).
49. G. Waterstraat, T. Fedele, M. Burghoff, H.-J. Scheer, G. Curio, Recording human cortical population spikes non-invasively—an EEG tutorial. *J. Neurosci. Methods* **250**, 74–84 (2015).
50. A. C. Meidahl *et al*., Synchronised spiking activity underlies phase amplitude coupling in the subthalamic nucleus of Parkinson's disease patients. *Neurobiol. Dis.* **127**, 101–113 (2019).
51. M. Stokes, E. Spaak, The importance of single-trial analyses in cognitive neuroscience. *Trends Cogn. Sci.* **20**, 483–486 (2016).
52. M. Lundqvist *et al*., Gamma and beta bursts underlie working memory. *Neuron* **90**, 152–164 (2016).
53. W. G. Coon, G. Schalk, A method to establish the spatiotemporal evolution of task-related cortical activity from electrocorticographic signals in single trials. *J. Neurosci. Methods* **271**, 76–85 (2016).
54. T. I. Regev, J. Winawer, E. M. Gerber, R. T. Knight, L. Y. Deouell, Human posterior parietal cortex responds to visual stimuli as early as peristriate occipital cortex. *Eur. J. Neurosci.* **48**, 3567–3582 (2018).
55. M. Haller *et al*., Persistent neuronal activity in human prefrontal cortex links perception and action. *Nat. Hum. Behav.* **2**, 80–91 (2018).
56. V. S. Zotev *et al*., SQUID-based instrumentation for ultralow-field MRI. *Supercond. Sci. Technol.* **20**, S367–S373 (2007).
57. J. Clarke, M. Hatridge, M. Mössle, SQUID-detected magnetic resonance imaging in microtesla fields. *Annu. Rev. Biomed. Eng.* **9**, 389–413 (2007).
58. T. Fedele, H. J. Scheer, M. Burghoff, G. Curio, R. Körber, Ultra-low-noise EEG/MEG systems enable bimodal non-invasive detection of spike-like human somatosensory evoked responses at 1 kHz. *Physiol. Meas.* **36**, 357–368 (2015).
59. H. C. Seton, J. M. S. Hutchison, D. M. Bussell, Liquid helium cryostat for SQUID-based MRI receivers. *Cryogenics* **45**, 348–355 (2005).
60. P. Welch, The use of fast fourier transform for the estimation of power spectra: A method based on time averaging over short, modified periodograms. *IEEE Trans. Audio Electroacoust.* **15**, 70–73 (1967).
61. M. Valencia, M. Alegre, J. Iriarte, J. Artieda, High frequency oscillations in the somatosensory evoked potentials (SSEP's) are mainly due to phase-resetting phenomena. *J. Neurosci. Methods* **154**, 142–148 (2006).
62. R. A. Brown, M. L. Lauzon, R. Frayne, A general description of linear time-frequency transforms and formulation of a fast, invertible transform that samples the continuous S-transform spectrum nonredundantly. *IEEE Trans. Signal Process.* **58**, 281–290 (2010).
63. R. A. Brown, R. Frayne, A fast discrete S-transform for biomedical signal processing. *Annu Int Conf IEEE Eng Med Biol Soc* **2008**, 2586–2589 (2008).
64. B. Efron, R. J. Tibshirani, *An Introduction to the Bootstrap* (CRC, 1994).
65. J. P. Romano, M. Wolf, Efficient computation of adjusted p-values for resampling-based stepdown multiple testing. *Stat. Probab. Lett.* **113**, 38–40 (2016).
66. C. Tallon-Baudry, O. Bertrand, Oscillatory gamma activity in humans and its role in object representation. *Trends Cogn. Sci.* **3**, 151–162 (1999).
67. O. David, J. M. Kilner, K. J. Friston, Mechanisms of evoked and induced responses in MEG/EEG. *Neuroimage* **31**, 1580–1591 (2006).